Geotechnical Aspects of Underground Construction in Soft Ground – Viggiani (ed)
© 2012 Taylor & Francis Group, London, ISBN 978-0-415-68367-8

Numerical simulation of long-term twin-tunnel behaviour at St James's park

R.G. Laver
AECOM, Hong Kong

K. Soga
Department of Engineering, University of Cambridge, Cambridge, UK

ABSTRACT: The twin-tunnel construction of the Jubilee Line Extension tunnels beneath St James's Park was simulated using coupled-consolidation finite-element analyses. The effect of defining different permeabilities for the final consolidation stage was investigated, and the performance of a fissure softening model was also evaluated. The analyses suggested an unexpectedly high permeability anisotropy for soil around the tunnel crown, possibly due to stress-induced permeability changes, or low-permeability laminations. Also, the permeability profile and lining conductivity were found to differ between the tunnels. Inclusion of the fissure model gave a narrower settlement trough, more alike that in the field, by preferentially softening simple shear behaviour. Long-term settlements at the site continue to increase at an unexpectedly high rate, suggesting the possibility of creep or unexpected soil softening during excavation.

1 INTRODUCTION

The impact of long-term changes after tunnel construction has attracted increasing interest. At the surface, continuing movements after excavation can cause further damage to buildings (Harris 2002), whilst below the surface, lining distortion and degradation is presenting a safety hazard for ageing metro systems. An understanding of the long-term behaviour of tunnels is urgently needed before these problems can be mitigated effectively.

Wongsaroj (2005) conducted a parametric study to investigate factors influencing the long-term behaviour of a single tunnel, through a series of coupled stress–pore pressure finite-element analyses.

To validate his analyses, he simulated the construction of the Jubilee Line Extension (JLE) twin tunnels beneath St James's Park, London, (1995–1996) and compared results to the monitoring data reported by Nyren (1998). To validate the long-term response, the resulting consolidation period was also simulated.

However, Wongsaroj executed only single-tunnel analyses, so that each tunnel was excavated in greenfield initial conditions; twin-tunnel interaction was therefore not accounted for.

This paper presents the simulation of twin-tunnel construction at St James's Park using coupled finite-element analyses, to account for interaction between the tunnels.

The simulation served to validate a parametric study investigating the long-term behaviour of twin tunnels; this study is described in Laver (2010).

The analyses also provided an opportunity to trial a new fissure model, outlined in Laver & Soga (2011). The fissure model was developed in response to two key observations from recent laboratory test data on London Clay (Hight et al. 2007): softening on fissures in triaxial extension tests, and softer behaviour for torsional shearing modes in the Hollow Cylinder Apparatus (HCA).

The twin-tunnel simulation of St James's Park also enabled the effect of different permeabilities to be assessed.

During the consolidation stage following construction of the first tunnel, Wongsaroj (2005) trialled different distributions of soil and lining permeability to match settlements and pore pressures in the field. To do this, he assigned different permeabilities to different strata, and also varied the permeability around the lining circumference.

Initially, the best-fitting soil and lining permeabilities found by Wongsaroj were applied in the twin-tunnel analyses of St James's Park. However, this resulted in poor replication of the final consolidation period—after construction of both tunnels—a period which Wongsaroj did not simulate. Four further combinations of soil and lining permeability were therefore trialled to match the field data better.

2 SITE DESCRIPTION

The Jubilee Line Extension beneath St James's Park consisted of two tunnels; one running westbound, and the other eastbound. More details about the site and monitoring can be found in Nyren (1998).

2.1 *Construction*

The twin 4.85 m-diameter running tunnels were excavated using backhoes in open-face shields, leading to volume losses of 3.3% and 2.9% respectively for westbound and eastbound tunnels.

The instrumentation was installed along a plane perpendicular to the tunnels; Figure 1 illustrates the instrumented section in elevation.

At 31 m depth, the advancement of the deeper westbound tunnel past the instrument plane was followed 256 days later by the 21 m-deep eastbound tunnel. Being diagonally juxtaposed in elevation, the tunnels were separated by 21.5 m in plan. Unlike its perpendicular crossing with the eastbound tunnel, the instrument plane intersected the westbound tunnel at an angle of around 80.

The lining was erected from unbolted concrete segments, which were expanded against the soil by inserting wedge-shaped key segments at knee level.

2.2 *Instrumentation*

The instrumentation included 24 Surface Monitoring Points (SMPs), providing 3-D surface displacements. Subsurface horizontal and vertical displacements were monitored by nine electrolevel inclinometer holes and eleven extensometer arrays. Five piezometers installed above the tunnels and four spade cells at eastbound tunnel axis level gave pore pressures and horizontal stresses.

2.3 *Geology & hydrogeology*

Topsoil and sandy man-made fill (Made Ground) at the site is underlain by sandy Alluvium and coarse to fine flint gravel (Terrace Gravel) to around 6–8 m Below Ground Level (BGL). Beneath this, London Clay extends to over 40 m depth, successively giving way to the Lambeth Group, Thanet Sands and Chalk bedrock.

Two aquifers persist across London: a deep aquifer in the Thanet Sands and Chalk below the London Clay and Lambeth Group, and a perched aquifer in the Terrace Gravels, recharged by precipitation and from the river Thames.

The pore pressure profile shown in Figure 2 nearby the site indicated a water table rising to about 5 m BGL. However, the sub-hydrostatic pore pressures towards the base of the London Clay indicated slight underdrainage from the deeper aquifer below.

Water strikes in several boreholes suggested the presence of water in claystone and sand partings.

3 ANALYSIS DETAILS

3.1 *Modelling procedures*

Twin-tunnel construction was simulated using the finite-element package ABAQUS. The simulation was divided into four stages: (i) westbound tunnel excavation, (ii) consolidation during the rest period, (iii) eastbound tunnel excavation, and (iv) consolidation until steady-state.

The two excavation stages were modelled with 3-D meshes for accurate replication of the excavation process. The mesh used is pictured in Figure 3. The lateral boundaries were located sufficiently distant to make boundary effects negligible. Data

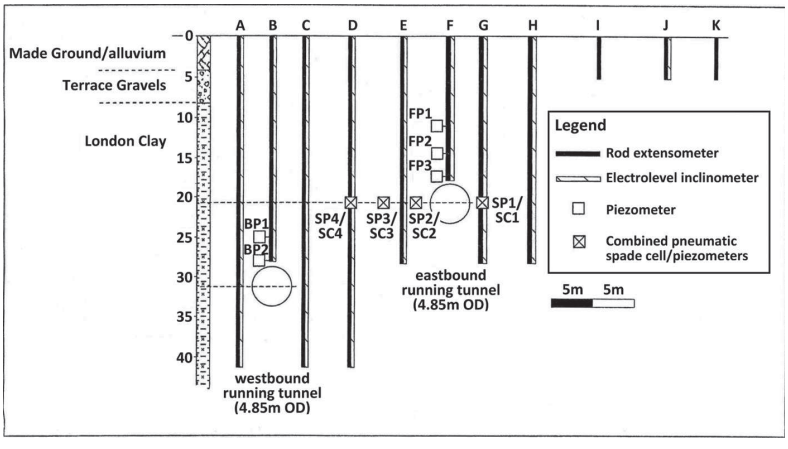

Figure 1. Elevation of instrumentation layout at St James's Park (after Nyren, 1998).

was extracted at a plane through which the tunnel was excavated, representing the instrument plane at St James's Park.

The two consolidation stages were modelled with 2-D meshes to reduce computational time. The 2-D meshes were defined with the same geometry as the instrument plane of the 3-D meshes.

By the end of each excavation analysis, a plane-strain condition had been reached on the instrument plane of the 3-D mesh. All data on the plane necessary to continue the analysis was then mapped to the 2-D mesh to model the ensuing consolidation during the rest period. Similarly, at the end of this stage, which lasted 256 days, data from the 2-D mesh was mapped onto the entire length of the 3-D mesh ready to model the eastbound excavation.

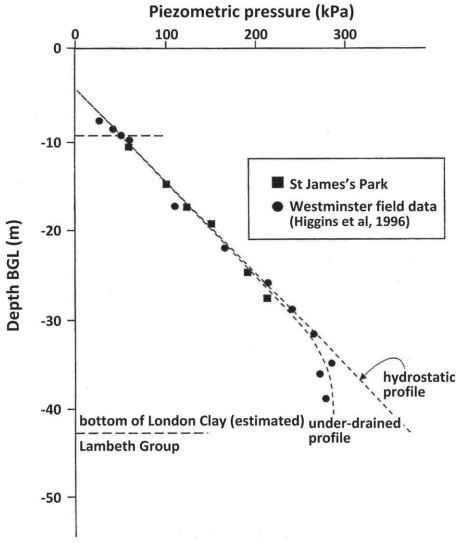

Figure 2. Pore pressure profile at St James's Park (after Nyren, 1998).

Excavation was progressed by removing soil elements and activating lining elements in 2 m lengths. A 6 m unsupported length for the tunnel heading was assumed, to match field observations (Nyren 1998). The speed of excavation simulated the rate of advance at St James's Park, progressing at 1.6 m per hour.

A linear elastic model was applied to the tunnel lining to model concrete, with $E = 28$GPa, $\upsilon = 0.15$ and $\rho = 2400$ kg m^{-3}, and the actual lining thickness of 0.2 m was adopted.

To reduce computational time, 8-node linear elements were mainly used, with 20-node reduced-integration quadratic elements only in a region immediately surrounding the tunnel, for a smoother pore pressure response. The tunnel lining was modelled with 8-node quadratic continuum shell elements. The lining and soil elements shared the same nodes at the tunnel boundary, thus simulating no-slip contact.

All analyses restricted out-of-plane displacements on the vertical boundaries, whilst displacements at the model base were fixed. Pore pressures were maintained at the ground surface and base of the model to locate the water table at 5 m below the ground surface, defining +50 kPa at the base to impart slight under-drainage to the hydrostatic profile. During the consolidation stages, a drainage-only seepage condition was applied around the tunnel boundary so that pore fluid could flow only into the tunnel, rather than out of it.

3.2 *Constitutive model*

Figure 3 illustrates the representative soil profile—the same used by Wongsaroj (2005)—derived by extrapolating borehole logs from ground investigations (Nyren 1998, Standing & Burland 1999). The stratum 'Made Ground' also includes the underlying Alluvium too.

The constitutive model formulated by Wongsaroj (2005) was adopted to model all soil strata. Building upon a critical-state foundation,

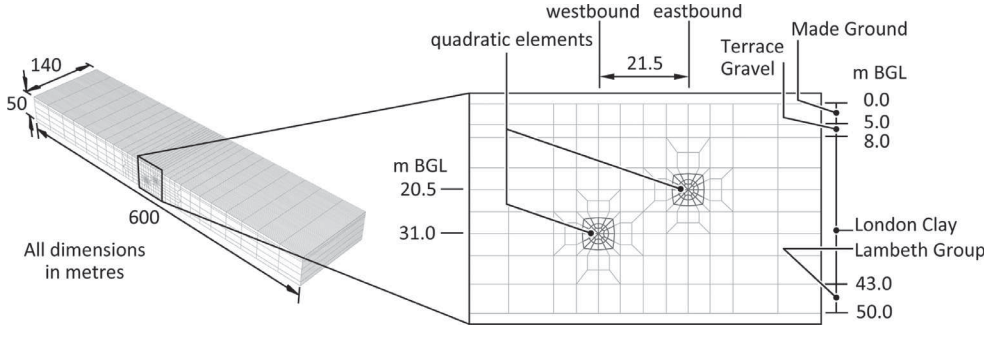

Figure 3. Geometry of 3-D mesh for twin-tunnel analyses.

Wongsaroj incorporated features from previous constitutive models.

The Modified Cam Clay (MCC) yield surface (Wheeler 1997) was adopted, allowing strength anisotropy to be modelled by rotating the yield surface. The equation of its axis is given by $s_{ij} = p' \beta_{ij}$, such that the tensor β_{ij} describes the rotation. The yield surface grows according to the plastic volumetric strain increment $d\varepsilon_v^p$:

$$dp'_0 = \frac{1+e}{e(\rho_c - \rho_r)} p'_0 \, d\varepsilon_v^p \tag{1}$$

where ρ_c as the gradient of the normal compression line, ρ_r that of the swelling line, p'_0 the intercept of the initial yield surface with the hydrostatic axis and e is the void ratio.

Wongsaroj combined elastic and plastic behaviour within the yield surface by implementing the sub-load surface of Hashiguchi & Chen (1998). This surface is geometrically similar to the yield surface, but scaled down by a factor R so that it passes through the current stress point. Its growth is related to its relative size, such that dR is a function of R:

$$dR = u_1 \left(\frac{1}{R^m} - 1 \right) \left\| d\varepsilon^p \right\| \tag{2}$$

where $d\varepsilon^p$ is the plastic strain increment, and u_1 and m are material constants.

Failure in the π-plane followed that proposed by Matsuoka & Nakai (1985).

Wongsaroj adopted a cross-anisotropic elastic stiffness matrix. Small-strain stiffness degrades as formulated in the MIT-S1 model of Pestana (1994). Formulated in log e–log p' space, the swelling gradient ρ_r degrades according to:

$$\rho_r = \frac{1 + \omega_s \xi_s}{C_b} \left(\frac{p'}{p_a} \right)^{\frac{1}{2}} + D\left(1 - \xi^r\right) \tag{3}$$

The constant p_a is the atmospheric pressure, whilst C_b, ω_s, D and r are material constants. The variables ξ and ξ_s are dimensionless distances in stress space since the last stress reversal, defined along the hydrostatic axis and in the deviatoric plane respectively.

The dimensionless distances ξ and ξ_s are reset and the initial stiffness is restored when the stress reverses. A stress reversal is defined according to Pestana (1994), by the scalar product of the current strain increment vector with the vector of accumulated strains since the last reversal. Thus, a negative product defines a change in strain direction.

The soil parameters applied to each stratum are summarised in Table 1. The initial preconsolidation pressure p'_0 varied linearly with depth: varying from 1000 kPa at the surface to 1080 kPa at 8 m depth, then increasing stepwise to 3000 kPa before increasing to 3420 kPa at 50 m depth. A bulk unit weight of 20 kN m^{-3} was applied to all strata. The derivation of these parameters is detailed in Laver (2010).

3.3 *Fissure softening model*

For London Clay, fissure softening was trialled by incorporating a fissure model into the constitutive model formulated by Wongsaroj (2005).

The fissure model assumes that fissures only exist on sub-horizontal and sub-vertical planes, within an inclination of ±16° from the horizontal and vertical directions respectively. Fissures in London Clay have been observed to pre-dominate at these orientations (Skempton et al. 1969).

Softening on these fissures is initiated when a critical friction angle of 11.5° is exceeded on these planes. Softening is implemented by applying a reduction factor to all components of the elastic stiffness matrix isotropically. The reduction factor ramps gradually down from unity to a minimum value as the friction angle rises above the critical value; the range over which this happens was set as 1.5°.

The minimum value of reduction factor, ζ_{min}, is dependent upon the element size to correctly account for the localisation of softening. The relation is given by:

Table 1. Soil parameters applied to strata.

	Stratum			
Parameter	Made ground	Terrace gravel	London clay	Lambeth roup
v_{vh}	0.2	0.2	0.015	0.2
v_{hv}	0.2	0.2	0.04	0.2
v_{hh}	0.2	0.2	0.12	0.2
G_{hh}/G_{vh}	1	1	1.5	1
C_b	100	400	300	900
ω_s	15	15	10	50
ρ_c	0.2476	0.556	0.3	0.37
D	0	0	0.05	0.05
r	0	0	2	2
u_1	100	100	300	100
m	0.1	0.1	0.05	0.1
M	0.984	1.418	0.814	1.07
β_{vv}	0	0	0.1	0
β_{hh}	0	0	–0.05	0
e_0	0.65	0.5	0.7	0.65
K_0	0.6	0.4	1.2	1.2

$$\zeta_{\min} = \frac{1}{1 + \dfrac{f_{\text{fiss min}}}{C_{\text{el}}}} \tag{4}$$

where C_{el} is a characteristic element length. The fissure property $f_{\text{fiss min}}$ was set as 3.6, determined by fitting to laboratory tests (Laver & Soga 2011).

3.4 *Analyses performed*

Six analyses were performed to investigate the effect of fissure softening and the choice of soil and lining permeabilities. In all analyses, Wongsaroj's soil and lining permeabilities were applied during the rest period between westbound and eastbound excavations.

Alternative permeabilities were only trialled in the final consolidation phase to avoid modelling the computationally expensive eastbound excavation for each trial. The six analyses were:

1. **MODFW** adopts Wongsaroj's constitutive model with fissure softening incorporated, and his choice of soil and lining permeabilities. His soil permeability profile is presented in Figure 4 and is detailed in Table 2, whilst his lining conductivity is represented by the westbound tunnel in Figure 5. The units of London Clay in Table 2 were located from borehole data collected at St James's Park by Standing & Burland (1999).
2. **MODFS1** same as MODFW, but with both kv and kh for Unit A3ii (20.5 m–28 m BGL) halved during the final consolidation.
3. **MODFS2** same as MODFS1, but with both kv and kh for Unit B2 (8 m–20.5 m BGL) reduced tenfold during the final consolidation.
4. **MODFS3** same as MODFS1, but with only k_v for Unit B2 reduced tenfold during the final consolidation.

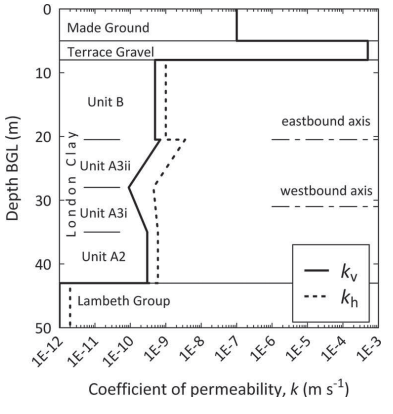

Figure 4. Permeability profile for analyses MODFU & MODFW.

Table 2. Permeability profile for analyses MODFU & MODFW.

	Depth	k_v	k_h
Stratum	m	m s^{-1}	m s^{-1}
Made ground	0–5	5×10^{-7}	5×10^{-7}
Terrace gravel	5–8	1×10^{-4}	1×10^{-4}
London clay			
Unit B2	8–20.5	5×10^{-10}	1×10^{-9}
Unit A3ii	20.5–28	7×10^{-10} to 9×10^{-11}	3.5×10^{-10} to 4.5×10^{-10}
Unit A3i	28–35	9×10^{-11} to 3×10^{-10}	4.5×10^{-10} to 6×10^{-11}
Unit A2	35–43	3×10^{-10}	6×10^{-10}
Lambeth group	43–50	5×10^{-12}	1×10^{-12}

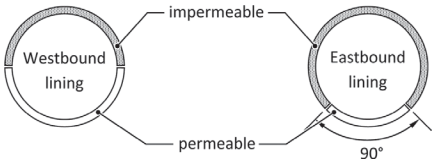

Figure 5. Lining permeabilities for analysis MODFT.

5. **MODFT** same as MODFW, but with the permeable region below the tunnel axis reduced for the eastbound tunnel, as shown in Figure 5.
6. **MODUT** adopts the same permeabilities as MODFT, but with Wongsaroj's unmodified constitutive model.

In trials MODFS1–3, soil permeabilities were rede-fined for the final consolidation stage, so that these trials were not entirely realistic. These trials were conducted purely to investigate the effect of permeability during final consolidation.

4 RESULTS AND DISCUSSION

4.1 *Effect of permeability*

Figures 6 and 7 show vertical displacements due to consolidation and pore pressures around the eastbound tunnel 371 days after its completion. The figures highlight the inadequacy of Wongsaroj's permeabilities (MODFW) to simulate the final consolidation stage:

(i) consolidation below axis level is overestimated by 25%, (ii) slight swelling above the tunnel is not replicated, and (iii) pore pressures above the crown recover to significantly lower values than in the field.

The analyses trialling alternative permeabilities sought to improve the replication. Trials MODFS1

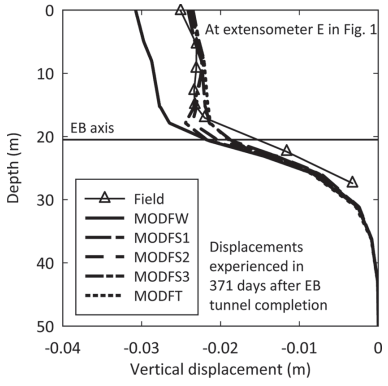

Figure 6. Profiles of vertical displacements adjacent to eastbound tunnel developed in first 371 days after its completion.

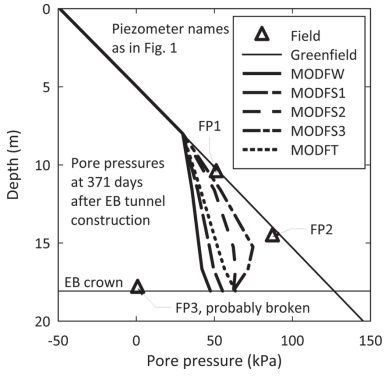

Figure 7. Pore pressure profiles at centreline of eastbound tunnel 371 days after its completion.

and MODFT both successfully reduced the consolidation below the springline to a realistic level. Both trials achieved this by reducing tunnel inflow below axis level in two different ways: MODFS1 reduced the permeability of the stratum encompassing the lower half of the tunnel (Unit A3ii), whilst MODFT reduced the conductivity of the lining itself below the spring-line. The fact that adjusting either the soil or the lining conductivity gave the same improvement highlights the uncertainty associated with backanalysing permeability values from field data.

However, both trials failed to replicate the swelling region above the crown and the recovery of pore pressures here. To overcome this, trials MODFS2 and MODFS3 reduced the permeability of the stratum encompassing the upper half of the tunnel (Unit B2). Trial MODFS2 maintained the same ratio between vertical and horizontal permeabilities, whilst trial MODFS3 reduced only the vertical permeability, giving $k_h/k_v = 20$.

Figure 6 shows that both trials reproduced the swelling zone above the crown. However, trial MODFS3 fitted the recovery of pore pressures significantly better in Figure 7.

The horizontal permeability (10^{-10} m s^{-1}) adopted for MODFS2 is still realistic, and within the range for Unit B2 (Hight et al. 2007). However, the permeability anisotropy ratio in trial MODFS3 is unexpectedly high for London Clay; two possible explanations for this are:

- Unit B2 may have a high in-situ anisotropy due to laminations. Nyren (1998) reported that clay-stone bands were encountered in 75% of boreholes sunk around St James's Park. The clay-stone would be less permeable than the surrounding clay, and would reduce the vertical permeability, whilst maintaining the horizontal permeability.
- The permeability of Unit B2 might have evolved due to tunnelling stress changes. The extension stress path above the crown might have closed vertical flow paths, but opened horizontal ones. Similar swelling and pore pressure recovery was also observed above the westbound tunnel crown (Nyren 1998)—founded instead in Unit A3i—suggesting stress-related permeability change to be the primary cause, rather than laminations in the strata.

Also, the need to modify soil permeabilities to match the field data for the final consolidation phase suggests that the permeability profile varies transversely between the two tunnels.

4.2 *Performance of fissure model*

Figure 8 compares normalised settlement troughs from trials MODUT and MODFT to assess the performance of the fissure model in replicating

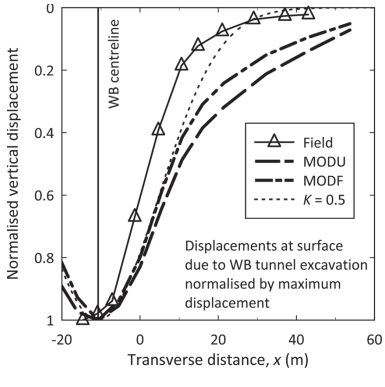

Figure 8. Surface settlement troughs due to westbound tunnel excavation.

the westbound tunnel excavation. Trials MODUT and MODFT both adopt the lining permeabilities shown in Figure 5; this improved the modelling of consolidation below the eastbound tunnel without the need to redefine soil permeabilities for the final consolidation.

The figure shows that both trials produce significantly wider troughs than those in the field, even though the trough at St James's Park is unusually narrow—with $K = 0.35$ (Nyren 1998) instead of $K = 0.5$, as expected for clay (Mair et al. 1993).

Despite this, comparison of trials MODUT and MODFT demonstrates that fissure softening helped to simulate a narrower trough. This is because the fissure model preferentially softened behaviour in simple shear compared with other shearing modes.

Figure 9 identifies different shearing modes during tunnel excavation, showing that simple shear modes are active between the tunnel and the ground surface. Softer behaviour in these modes for trial MODFT reduced the spread of settlement, resulting in a narrower trough.

The fissure model provides a realistic method to make the trough narrower for fissured clays like London Clay, even though the trough is still too wide. However, narrower troughs are also observed for un-fissured clays in the field, e.g. Guedes de Melo & Santos Pereira (2000).

For unfissured clays, an alternative to simulating softer shear behaviour without invoking fissure softening would be to apply the tangential stress rate (Hashiguchi & Tsutsumi 2001). Here, plastic strains evolve according to the component of the stress increment tangential to the yield surface, in addition to the normal component. However, the implementation is currently limited to isotropic elasticity; generalisation to anisotropic elasticity would render it practically useful for modelling clays in large-scale numerical analyses.

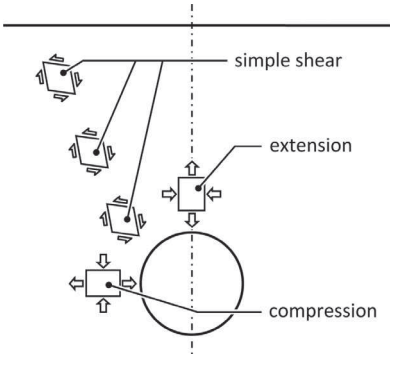

Figure 9. Shearing modes induced by tunnel excavation.

4.3 *Replication of long-term settlements*

Figures 10 and 11 present the long-term settlements developed since completion of the eastbound tunnel, showing variation with time and settlement troughs respectively.

Figure 10 shows that predicted settlement rates agree well with the field data in the first few years. After this however, settlement in the field continues to develop at an appreciable rate, showing little signs of decaying, even after 10 years.

This could be due to the overestimation of coefficient of consolidation c_v in the field; also presented on Figure 10 is an analysis adopting back-analysed values of stiffness and permeability; the stiffness parameter C_b for London Clay was reduced from 300 to 100, whilst both horizontal and vertical permeabilities of Unit A3ii—encompassing the permeable portion of the eastbound lining—were

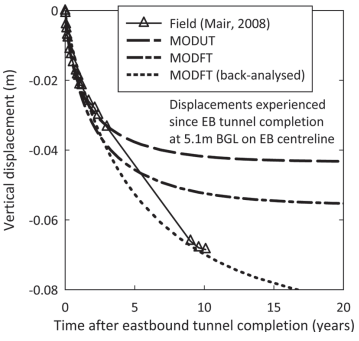

Figure 10. Development of long-term settlement with time after eastbound tunnel completion.

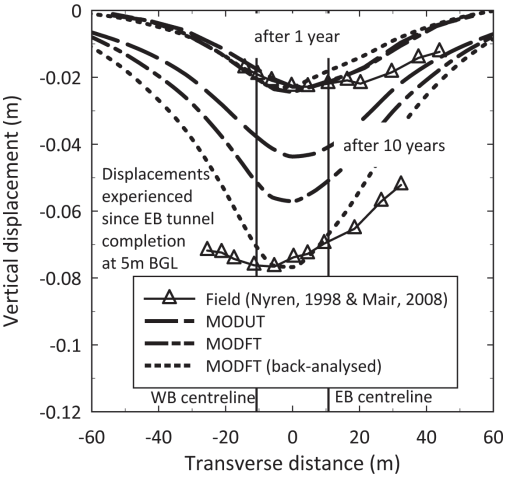

Figure 11. Long-term settlement troughs after eastbound tunnel completion.

halved. This demonstrates that the field data can be fitted by reducing c_v; whether the back-analysed stiffness and permeability are realistic for the site remains to be ascertained. It should also be noted that the back-analysed plot does not represent a realistic simulation: the stiffness and permeability were only modified in the final consolidation stage; the plot is therefore only demonstrative.

In Figure 11, simulated trough widths are roughly similar to those in the field; differences can be attributed to transverse variation in the permeability profile.

5 CONCLUSIONS

This paper presented the simulation of the JLE twin-tunnel construction below St James's Park using coupled-consolidation finite-element analyses.

The analyses investigated the effect of defining different soil and lining permeabilities on the final consolidation phase. A different soil permeability profile best-matched the consolidation stage after eastbound excavation than that after the west-bound one, highlighting a transverse variation of permeability in the field.

Defining a high degree of permeability anisotropy for the stratum encompassing the eastbound tunnel crown resulted in a more realistic pore pressure response. In the field, the high anisotropy might either be due to stress-induced permeability changes or to the presence of claystone laminations. These findings highlight the need for more data on field permeabilities, particularly on how permeability evolves with stress change. The findings also highlight the sensitivity of long-term behaviour to both soil and lining permeabilities.

The analyses also assessed the performance of the fissure model in simulating tunnel excavation. The analysis incorporating the fissure model successfully produced a narrower settlement trough—more alike that in the field—by preferentially softening behaviour in simple shear. The fissure model therefore provides a realistic method of replicating a narrow settlement trough in fissured clays. For unfissured clays, similar behaviour might be achievable by incorporating the tangential stress rate (Hashiguchi & Tsutsumi 2001).

The simulations highlighted that settlements in the field continue to develop at an unexpectedly high rate, which can be attributed to an overestimation of stiffness and permeability in the field.

REFERENCES

Guedes de Melo, P.F.M. & C. Santos Pereira (2000). The role of k_0 value in numerical analysis of shallow tunnels. In Kusakabe, Fujita, and Miyazaki (Eds.), *Proc. Int. Symp. Geotech. Aspects of Underground Construction in Soft Ground*, Rot-terdam, pp. 379–384. Balkema.

Harris, D.I. (2002). Long term settlement following tunnelling in overconsolidated London Clay. In *Proc. 3rd Int. Symp. Geotech. Aspects of Underground Construction in Soft Ground*, Toulouse, pp. 393–398.

Hashiguchi, K. & Z.P. Chen (1998). Elastoplastic constitutive equation of soils with the subloading surface and the rotational hardening. *Int. J. Numer. Anal. Methods in Geomechanics 22*, 197–227.

Hashiguchi, K. & S. Tsutsumi (2001). Elastoplastic constitutive equation with tangential stress rate effect. *Int. J. Plast. 17*, 117–145.

Hight, D.W., A. Gasparre, S. Nishimura, N.A. Minh, R.J. Jardine, & M.R. Coop (2007). Characteristics of the Lon-don Clay from the Terminal 5 site at Heathrow Airport. *Géotechnique 57* (1), 3–18.

Laver, R.G. (2010). *Long-term behaviour of twin tunnels in clay*. Ph. D. thesis, University of Cambridge.

Laver, R.G. & K. Soga (2011). Performance of two constitutive models for fissures in clay. In *Int. Symp. on Deformation Characteristics of Geomaterials*, Seoul, Korea. in press.

Mair, R.J., R.N. Taylor, & A. Bracegirdle (1993). Subsurface settlement profiles above tunnels in clays. *Géotechnique 43* (2), 315–320.

Matsuoka, H. & T. Nakai (1985). Relationship among Tresca, Mises, Mohr-Coulomb and Matsuoka-Nakai failure criteria. *Soils & Foundations 25*(4), 123–128.

Nyren, R.J. (1998). *Field measurements above twin tunnels in clay*. Ph. D. thesis, Imperial College of Science, Technology & Medicine, London.

Pestana, J.M. (1994). *A unified constitutive model for clays and sands*. Ph. D. thesis, Massachusetts Institute of Technology, Boston.

Skempton, A.W., R.L. Schuster, & D.J. Petley (1969). Joints and fissures in London Clay at Wraysbury and Edgware. *Géotechnique 19* (2), 205–217.

Standing, J.R. & J.B. Burland (1999). Report on ground characterisation to explain tunnelling volume losses in the West-minster area. Internal report, Imperial College of Science, Technology & Medicine, London.

Wheeler, S.J. (1997). A rotational hardening elasto-plastic model for clays. In *Proc. 14th Int. Conf. Soil Mech. & Foundation Engng.*, Volume 1, Hamburg, pp. 431–434.

Wongsaroj, J. (2005). Three-dimensional finite element analysis of short and long-term ground response to open-face tunnelling in stiff clay. Ph. D. thesis, University of Cambridge.